Illumination-dependent temperature coefficients of the electrical parameters of modern silicon solar cell architectures

Simon M.F. Zhang [a,*], Johannes P. Seif [a], Malcolm D. Abbott [a], Anh Huy Tuan Le [a], Thomas G. Allen [b], Ivan Perez-Wurfl [a], Ziv Hameiri [a]

[a] University of New South Wales, Sydney, NSW 2052, Australia
[b] King Abdullah University of Science and Technology, Thuwal 23955-6900, Saudi Arabia

ABSTRACT

Photovoltaic devices operate under a wide range of temperature and illumination conditions. While the temperature coefficients (TC) of crystalline silicon solar cells have been well-studied, there have been only a few investigations regarding the effect of illumination on TCs. In this study, the TCs of the main electrical parameters of various silicon solar cell technologies are first determined. The illumination spectrum dependence of the TC of the short-circuit current and the illumination intensity dependence of the TC of the open-circuit voltage are then investigated. For the latter investigation, a custom-designed temperature-dependent Suns-V_{OC} system is used. It is found that: (1) the TC of the short-circuit current measured using an A-rated spectrum may differ from the TC measured using the AM1.5G spectrum by up to 30%, (2) the TC of the open-circuit voltage of all technologies at 0.001 suns approximately doubles compared to at one-sun, and (3) silicon heterojunction cells seem to have the overall best TC performance at medium to high intensities.

1. Introduction

For the past four-and-a-half decades, the photovoltaics (PV) industry has been growing at an extraordinary rate: expanding from less than 1 MW in 1975 to close to 1 TW in 2020 with a learning rate of almost 24% [1]. Although the transition from the aluminum back surface field (Al-BSF) to the passivated emitter and rear contact (PERC) cells was completed only recently [1], several candidates for the next generation of commercial technologies are already under development [2]. The technologies receiving the most attention are silicon (Si) heterojunction (SHJ) [3] and tunnel oxide passivated contact (TOPCon) cells [4], which are predicted to gain significant market share within the next decade [1]. To advance the development of these cell structures and facilitate an eventual transition, it is critical to investigate their performance under the full range of field conditions. As PV systems are exposed to a wide range of temperatures (T), illumination spectra, and illumination intensities (φ), it is vital that such investigations consider all these parameters.

The temperature dependence of a solar cell is conventionally expressed in terms of the temperature coefficient (TC) of its major electrical parameters: open-circuit voltage (V_{OC}), short-circuit current density (J_{SC}), fill factor (FF), and efficiency (η). Numerous studies have used temperature-dependent current-voltage [I-V(T)] measurements to determine the TCs of crystalline Si (c-Si) cells [5–8] and modules [5,9, 10] under one-sun illumination. Others have determined the TCs of cells [11,12] and modules [13,14] under up to seven illumination intensities, as well as modules under field conditions [15]. Using the I-V(T) technique, Monokrousso et al. [12] found that the absolute TC_{Voc} ($TC_{Voc,abs}$) of multi-crystalline PERC cells becomes more negative by approximately 10% when reducing the light intensity from 1.1 suns to 0.1 suns. The same trend has also been reported by Tayyib et al. [11] for c-Si cells manufactured from upgraded metallurgical grade silicon, and Le et al. [16] found the same for TOPCon cells using temperature-dependent Suns-V_{OC} [Suns-V_{OC}(T)].

Only a few studies investigated the impact of the spectrum on TC. Green highlighted the dependence of TC_{Jsc} on the spectral distribution of illumination [17], stressing the increased photon absorption near the material bandgap (E_g) with increasing temperature. Osterwald et al. [18, 19] and Hishikawa et al. [20] measured the spectrum-dependent TC_{Jsc} of various c-Si cells and modules, confirming the predicted dominance of the bandgap effect as well as suggesting models to approximate the spectral dependence of the TC_{Jsc} of c-Si cells.

In comparison to I-V testers, the Suns-V_{OC} technique [21] utilizes a flash and records illumination intensity-voltage pairs without current flow and series resistance (R_S) effects, allowing hundreds of V_{OC} measurements across a wide range of intensities. Suns-V_{OC}(T) measurements, therefore, have a high potential to quickly determine the illumination-intensity-dependent TC_{Voc} [$TC_{Voc}(\phi)$] of PV cells over a wide range of intensities, with small intensity steps. This allows for deeper insight into the physical mechanisms of TC_{Voc}, which in most cases comprises the majority of TC_{η} [5,7,9,11,14–16]. Hence, the investigation of $TC_{Voc}(\phi)$ using Suns-V_{OC}(T) may have the potential for a significant step forward in the study into the temperature- and illumination-dependence of PV cell performance. At room temperature, Suns-V_{OC} measurements have been used in a wide range of applications, such as the calculation of R_S [22], the derivation of the injection-dependent lifetime [21,23], and the probing of Schottky contacts in solar cells [24]. However, until now, temperature-dependent Suns-V_{OC} [Suns-V_{OC}(T)] measurements have only been rarely used [16].

In this study, we first determine the TCs of the main electrical parameters of four types of solar cells: n-type SHJ, n-type TOPCon, n-type PERT (passivated emitter and rear totally diffused), and p-type PERC. We present these cells' I-V(T) performance under one-sun illumination and compare their TCs to reported values. We then investigate the spectral dependence of their TC_{Jsc}. Next, we study their $TC_{Voc}(\phi)$ using our newly developed Suns-V_{OC}(T) system that allows deeper insight into the physical mechanisms of TC_{Voc}.

2. Material and methods

Four commercial solar cell technologies are investigated in this study. All cells were fabricated using 6-inch Czochralski (Cz) monocrystalline Si wafers. The base resistivity (ρ) of the cells was determined by capacitance-voltage (C-V) measurements [25]. Table 1 provides the average and range of the electrical parameters of three sister cells from each technology measured under standard test conditions (STC). One representative cell from each technology is then selected for in-depth characterization. The highest reported efficiency for the large-scale production of commercial SHJ cells is 23.65% [26,27], and that of TOPCon is 23% [28]. Recent reports of mass-produced PERT cells are harder to find, however an industry-compatible batch of cells was demonstrated at an average efficiency of 23% [29]. For PERC, an average efficiency of 22.5% was reported [30]. As our investigated cells are within 1% of the industry state-of-the-art, the measured characteristics from this study and the conclusions drawn from these should be applicable to cells currently produced by the industry.

I-V(T) measurements were conducted using a Sinus-220 (WaveLabs) tester in the temperature range of 25–65 °C. Several measurements beyond the standard one-sun illumination sweep were performed at each temperature: illuminated I-V at half-sun, dark I-V, and Suns-V_{OC} in the illumination range of 0.05 suns to one-sun. TCs were extracted via linear regressions of the corresponding parameter to the applicable temperature range.

Suns-V_{OC}(T) measurements in the temperature range of 30–140 °C and illumination range of 0.001 suns to 19 suns were conducted using a custom-built tool from Sinton Instruments in which a temperature stage is integrated into the standard Suns-V_{OC} setup [16,31]. Since the size of the Suns-V_{OC}(T) temperature stage is smaller than 6-inch, four sister cells to the cells listed in Table I were cleaved into 10×10 cm^2 squares. The impact of this cleaving will be evaluated below. The Suns-V_{OC}(T) measurements were analyzed using a Python script written in-house, which uses the semiconductor package [32]. The extraction of m(V, T) was performed by calculating the local slope of V_{OC} as a function of the natural logarithm of the light intensity [33], using four adjacent points. I-V(T) measurements in the temperatures of 30 °C and 65 °C were also conducted for these cells. The base resistivity of these cleaved cells are displayed in Table I.

Temperature-dependent external quantum efficiency [EQE(λ, T)] measurements were conducted in the wavelength range of 300 nm to 1200 nm with 10 nm intervals using LOANA (pv-tools) in the temperature range of 25–80 °C. The obtained EQE(λ, T) spectra are then superimposed with the AM1.5G spectrum [34], as well as with the approximated AM1.5G spectra from the Sinus-220 system, to calculate the temperature-dependent J_{SC}. From this, the TC_{Jsc} can be obtained, in addition to the TC_{Jsc} directly extracted from the I-V measurements.

3. Results and discussion

3.1. Temperature-dependent I-V performance

The temperature dependence of the main electrical parameters as extracted from the I-V(T) measurements are shown in Fig. 1. They match the expected trends [17]: a small positive temperature dependence for J_{SC}, and negative temperature dependences for V_{OC}, FF, and efficiency. All trends are linear within this temperature range.

The relative magnitude of V_{OC} of the four cell structures is a result of the effectiveness of the suppression of recombination in each structure. The PERC cell, with the lowest voltage in the lot, features rear surface passivation based on charge control provided by an aluminum oxide (AlO$_x$) layer [35]. The PERT cell improves upon this by using an n-type bulk, which is tolerant of metal impurity and is less vulnerable to light-induced degradation [36], both of which increase recombination, hence lowering the voltage. The TOPCon cell further reduces rear side recombination by completely removing the metal/c-Si interface and using a stack of silicon dioxide and polysilicon layer as a passivating contact [37]. The SHJ removes both front and rear metal/c-Si interfaces altogether by utilizing hydrogenated amorphous Si (a-Si:H) layers which also provide excellent passivation [3,5].
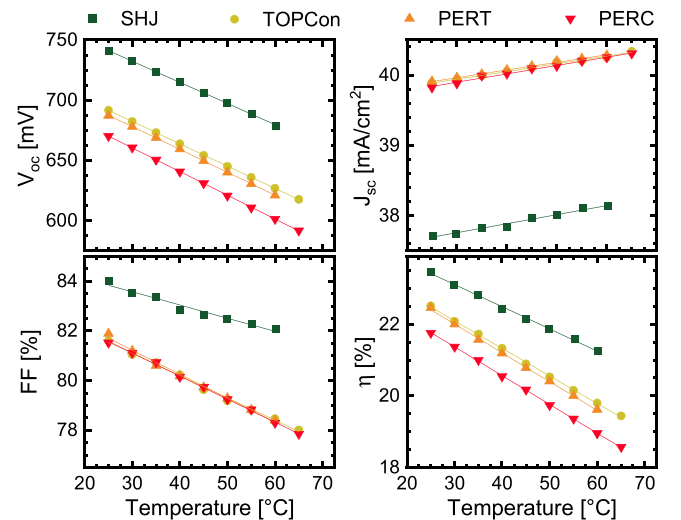
Table 1
Electrical parameters of the cells under STC.

Cell Type	Thickness [μm]	ρ [Ω•cm]	V_{OC} [mV]	J_{SC} [mA/cm^2]	FF [%]	η [%]
SHJ	150 ± 8	1.15	741 ± 1	37.7 ± 0.3	83.5 ± 0.5	23.4 ± 0.1
TOPCon	182 ± 5	1.59	692 ± 1	39.8 ± 0.2	81.7 ± 0.8	22.5 ± 0.4
PERT	172 ± 8	1.38	682 ± 5	39.8 ± 0.2	81.6 ± 0.3	22.2 ± 0.4
PERC	185 ± 8	0.70	670 ± 2	39.8 ± 0.1	81.2 ± 0.3	21.7 ± 0.1

Fig. 1. Performance of the different cell structures as a function of temperature obtained through I-V(T) measurements at one-sun.

The similar top layer sequences in the PERC, PERT, and TOPCon cells also give rise to similar photon absorption profiles, resulting in near-identical J_{SC} [38]. The SHJ cell, on the other hand, displays an approximately 5% lower J_{SC} due to parasitic absorption in the front transparent conductive oxide (TCO) and a-Si:H layers [3]. The latter layers absorb in similar wavelength ranges as the active bulk, and the former induces parasitic absorption due to the conflicting material qualities required by its dual functions of suppressing reflection and providing lateral carrier transport. In homojunction cells, in contrast, lateral carrier transport is provided by the electrons/holes collector while the anti-reflection coating (ARC) suppresses the reflection, making optimization possible without a tradeoff between these two.

FF is mainly a function of V_{OC}, R_S, and shunt resistance (R_{SH}) [38]. The approximately 2% absolute higher FF of the SHJ cell as compared to the homojunction cells is therefore likely due to its higher V_{OC}. The relatively low R_S (see Appendix A) of the PERC cell raises its FF to be similar to that of the TOPCon and PERT cells, despite its lower V_{OC}. As the investigated cells show a minimum R_{SH} of > 250 kΩ•cm^2 at 25 ℃, its effect on FF should be minimal. For SHJ cells, others have reported non-linear behavior of the FF at low temperatures [5,39]. This has been explained by the charge carriers' lack of energy to overcome the thermionic barriers at the heterojunctions at low temperatures [39,40]. When a thinner intrinsic a-Si:H [a-Si:H(i)] layer is used in the cells [8], tunneling becomes dominant at the c-Si/a-Si:H interface and the non-linearity is not observed at the temperatures considered in this report. This appears to be the case in the investigated SHJ cells.

Solar cell efficiency is the product of V_{OC}, FF, and J_{SC} (divided by the incoming one-sun power intensity). Here, the cell-to-cell trend in efficiency appears identical to that in V_{OC}, as the homojunction cells appear almost identical in J_{SC} and FF, and the SHJ cell's higher V_{OC} and FF compensate for its deficiency in J_{SC}.

3.2. Temperature coefficients at one-sun

TCs of the main electrical parameters are extracted from the I-V(T) measurements and presented in Fig. 2, which also includes results obtained by Haschke et al. [5] and Le et al. [16] for comparison. The TOPCon cell cited in [16] is a busbar-less MonoPoly™ cell onto which contacts were deposited for characterization. As this process changed the R_S of the cell, TC_{FF} and TC_η were not provided.
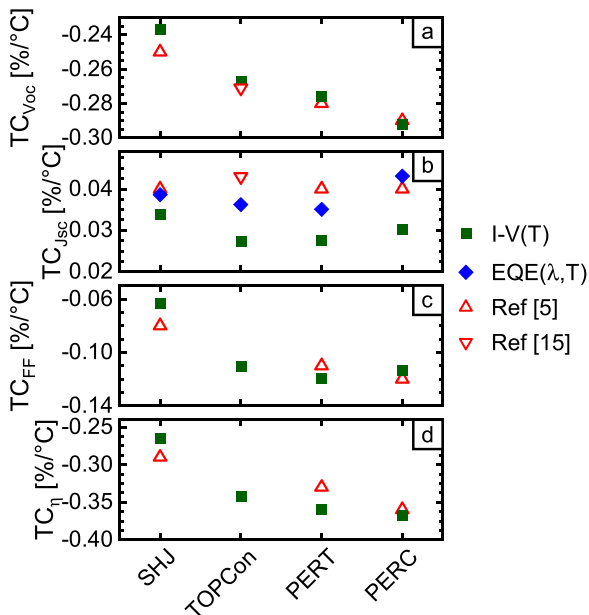

Fig. 2. Temperature coefficients of (a) V_{OC}, (b) J_{SC}, (c) FF, and (d) efficiency, obtained by I-V(T) and EQE(λ, T) measurements and normalized to 25 ℃.

Fig. 2(a) shows the TC_{Voc} of each cell at one-sun. The trend in the magnitude of the temperature coefficient is consistent with the trend in the magnitude of V_{OC} at 25 ℃ (see Eq. 3), in agreement with [17]. That is, a smaller V_{OC} corresponds to a more negative TC_{Voc}. The TC_{Voc} of our investigated cells agree well with the TC_{Voc} reported in [5] and [16], showing a maximum difference of approximately 5.5% relative.

Based on Fig. 2(b), it seems that the TC_{Jsc} of the investigated cells obtained using I-V(T) measurements are, on average, lower than the values reported by others by more than 25% relative. This difference is further investigated in Subsection C.

Comparing the TC_{FF} of each cell, the familiar trend of the SHJ being least negative and the other three cells having similar values is once again seen. Zhao et al. [41] suggested that for modern Si cells with high efficiency and R_{SH}, TC_{FF} can be divided into two components: one dependent on V_{OC} and TC_{Voc}, and one on R_S and TC_{Rs}:

$$TC_{FF} \approx (1 - 1.02FF_0)\left(TC_{Voc} - \frac{1}{T}\right) - \frac{R_S}{V_{OC}/J_{SC} - R_S}TC_{Rs} \tag{1}$$

where FF_0 is the FF of a cell assuming zero R_S and infinite R_{SH}, I_{SC} is the short-circuit current, and TC_{Voc} and TC_{Rs} have a unit of $℃^{-1}$. Based on the values of the relevant parameters, we estimate that R_S and TC_{Rs} account for less than 6% of TC_{FF} for all our investigated cells (see Appendix A). Hence, the marked difference between the SHJ and homojunction cells, as well as between our SHJ and the SHJ cell in [5] likely stems from the superior V_{OC} and TC_{Voc} of our SHJ cell.

TC_η is the sum of TC_{Voc}, TC_{Jsc}, and TC_{FF} [6]. As TC_{Voc} comprises over 64% of the sum of all TC magnitudes (see Appendix B) for all four cell structures, it dominates TC_η. This summation also explains the difference between the TCs of our cells and those presented in [5]: both the SHJ's higher TC and the PERT's lower TC can be observed in the other three parameters. Overall, the SHJ cell shows the best temperature performance with the single exception of TC_{Jsc} where it is second to the PERC cell. The strong performance of SHJ is in agreement with observations in [5,9].

3.3. Spectrum-dependent TC_{Jsc}

Fig. 2(b) highlights the existence of a significant gap between TC_{Jsc} obtained from our I-V(T) measurements and that previously reported. This section investigates this observed difference and explores its implications.

As Green et al. pointed out [17], TC_{Jsc} comprises two major components, one relating to the bandgap of the material, and one to the cell architecture and the resulting collection efficiency (f_c):

$$TC_{Jsc} = \frac{1}{J_{SC,ideal}} \frac{dJ_{SC,ideal}}{dE_g} \frac{dE_g}{dT} + \frac{1}{f_c} \frac{df_c}{dT} \tag{2}$$

where $J_{SC,ideal}$ is the current equivalent to the sum of all photons with energy greater than the bandgap in the incident spectrum.

In Si, the first term of Eq. (2) incorporates the phenomenon of bandgap narrowing (BGN) [42], where E_g decreases from 1.13 eV (1097 nm) at 25 ℃ to 1.11 eV (1117 nm) at 100 ℃ [43]. As this takes place, additional photons near the bandgap are absorbed, generating additional carriers, and increasing J_{SC}. This dynamic can be seen in Fig. 3(a), where EQE(λ, T) of the PERC cell broadens in the bandgap region (wavelength greater than approximately 900 nm) with increasing temperature. Similar observations can also be made regarding the other cell types (see Appendix C).

In Fig. 3(a), the EQE(T) at each wavelength shows a linear temperature dependence. Performing a linear regression and normalizing to the value at 25 ℃, we obtain a wavelength-dependent TC of the EQE [$TC_{EQE}(\lambda)$], plotted in Fig. 3(b). At shorter wavelengths, $TC_{EQE}(\lambda)$ is slightly negative with a small magnitude (no more than 0.02%/℃). As wavelength increases, $TC_{EQE}(\lambda)$ shows a slow increase, becoming
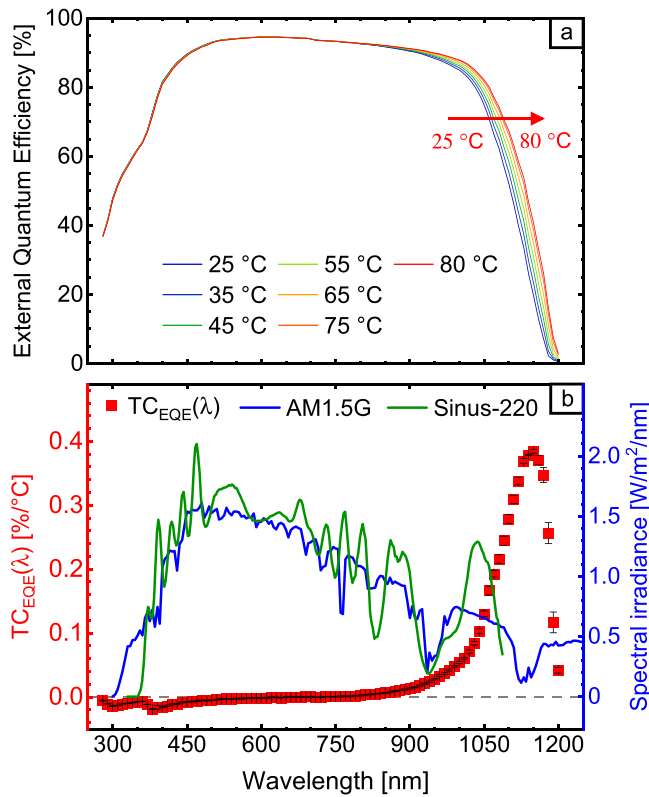
Fig. 3. Temperature-dependent spectral response of the PERC cell: (a) EQE(λ, T), and (b) TC$_{EQE}$(λ), the AM1.5G spectrum, and the Sinus-220′s AM1.5G-approximation spectrum.

positive near 650 nm, and beginning to increase rapidly at approximately 900 nm to reach the bandgap-related peak of 0.39%/°C at 1150 nm. This trend is replicated in the other structures (see Appendix C) and agrees with trends reported in [18–20].

As J$_{SC}$ is the spectral integral of the product of illumination intensity and EQE, the strong wavelength dependence of TC$_{EQE}$ indicates that TC$_{Jsc}$ measurements are highly sensitive to the spectral distribution of irradiance; that is, mismatches in the near-bandgap region will result in a significant difference in TC$_{Jsc}$. Using the measured EQE(λ, T) and the AM1.5G spectrum (plotted in Fig. 3(b) based on [34]), we calculated the J$_{SC}$ of each cell at each temperature, and therefore their TC$_{Jsc}$ under AM1.5G. As can be seen in Fig. 2(b) (blue diamonds), the calculated AM1.5G TC$_{Jsc}$ are similar to the literature values. Fig. 3(b) also displays the AM1.5G-approximation spectrum generated by the AAA-rated, light-emitting diode (LED)-based solar simulator featured in the Sinus-220 system. As can be seen, despite producing a relatively close match to AM1.5G for most of the spectrum, the simulator does not emit any radiation above approximately 1085 nm and therefore does not account for the majority of thel bandgap peak in TC$_{EQE}$(λ), producing a significantly underestimated TC$_{Jsc}$. In contrast, xenon lamp spectra [44] feature a closer match to AM1.5G in this long wavelength range, and hence a more accurate TC$_{Jsc}$ (see Appendix D).

Hence, the strong spectral dependence of TC$_{Jsc}$ requires the used solar simulator to provide a good spectral match to the desired spectrum, especially in the approximate range of 950 nm to 1200 nm. Note that those requirements are tighter than the requirements for J$_{SC}$ measurements which depend on EQE(λ) [instead of TC$_{EQE}$(λ)] which significantly reduces above 950 nm and therefore is less sensitive to spectral mismatch above this wavelength. Interestingly, the current requirements for a class A spectrum do not seem to support accurate TC$_{Jsc}$ measurements [45], as they only specify that of the full spectral range, 16.69 ± 4.17% of irradiance should fall between 900 nm and 1100 nm,

with no requirement beyond 1100 nm.

Furthermore, the spectral dependence of TC$_{Jsc}$ introduces additional complexities in current matching between the top and bottom cells in two-terminal tandem devices [46,47], where the bottom is often a c-Si cell [48]. One of the spectral mechanisms inducing changes in the bottom cell TC$_{Jsc}$ is well-known:

1) The temperature dependence of the top cell's bandgap will result in a changing spectrum of incident light to the bottom cell at each temperature [49]. Hence, in the case of a negative TC$_{Jsc}$ of the top cell (such as perovskites [50,51]) shorter wavelength photons will reach the bottom cell at higher temperatures (vice versa for a positive TC$_{Jsc}$ as in gallium arsenide [50]).

In addition to this well-known effect, the spectral dependence of TC$_{Jsc}$ highlights two further complications:

2) As the top cell blocks most of the short-wavelength incident light, the TC$_{Jsc}$ of the bottom cell will increase due to the exclusion of a spectral segment with smaller-than-overall TC$_{EQE}$(λ). For example, if all incident photons below 750 nm are blocked by the top cell (e.g. by perovskite), the absolute TC$_{Jsc}$ of the investigated PERC cell will increase by approximately 4.3% relative, resulting in a J$_{SC}$ increase of approximately 0.04 mA/cm^2 at 75 °C.

3) As temperature variations induce changes to the spectral range blocked by the top cell, the TC$_{Jsc}$ of the bottom cell will change due to the inclusion (or exclusion) of a spectral segment with smaller-than-overall TC$_{Jsc}$. As only a small spectral segment is involved, this mechanism should only have a fraction of the impact that (2) has on the J$_{SC}$ at the operating temperatures.

From the above descriptions, it can be inferred that under typical spectra and cell materials conditions the impact of (1) will be much larger than the combined effect of (2) and (3), and the impact of all three cannot be neatly separated. Nevertheless, it is important to note the existence of all three mechanisms for the sake of a more complete understanding of current matching, as well as for modeling purposes.

### 3.4. Illumination-intensity-dependent TC$_{Voc}$

In addition to the wide range of temperatures, PV modules also operate in diverse illumination conditions. Hence, in addition to TCs at one-sun, it is also important to obtain the illumination intensity dependence of these TCs. As TC$_{Voc}$ accounts for more than 60% of TC$_\eta$ (see Appendix B), obtaining TC$_{Voc}$(φ) can reveal important information. As indicated previously, we use the Suns-V$_{OC}$(T) technique to obtain TC$_{Voc}$(φ) at 100 points throughout 0.001 suns to 19 suns. Due to the size of the heating stage in our Suns-V$_{OC}$(T) system, four laser-cleaved 10 × 10 cm^2 samples from sister cells to those measured by the I-V(T) are used in this section.

To ensure the validity of the results obtained from the cut cells [using the Suns-V$_{OC}$(T) system], the extracted TC$_{Voc}$ are compared to the TC$_{Voc}$ obtained from the full cells [I-V(T)]. As shown in Fig. 4, at both one-sun and half-sun illumination intensities, the TC$_{Voc}$ obtained from the cut and full cells are within 3.5% for the homojunction cells confirming the reliability of the quantitative measurements based on the cut homojunction cells. While the larger difference of approximately 9% for the SHJ cell raises some concerns, compared to the overall change across the temperature range, 10% has no significant impact on the studied trends.

For all investigated cells, TC$_{Voc}$ becomes more negative as illumination intensity decreases. This trend can be explained by TC$_{Voc}$'s aforementioned dependence on V$_{OC}$. The inset to Fig. 4 presents the cells' TC$_{Voc,abs}$ as a function of V$_{OC}$. Their slope can be described by the following equation [17]:

$$TC_{V_{OC},abs} = \frac{dV_{OC}}{dT} = \frac{V_{OC}}{T} - \frac{E_{g0} + \gamma k_B T}{qT} \tag{3}$$
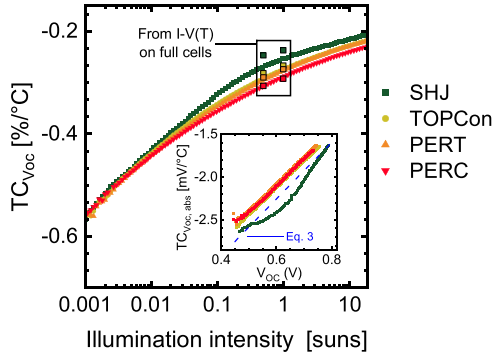
Fig. 4. $TC_{Voc}(\phi)$ normalized to 30 °C, as a function of illumination intensity. Points highlighted at one-sun and half-sun were obtained through I-V(T) measurements of the full cells. Inset: Absolute TC_{Voc} as a function of V_{OC} at 30 °C, where $\gamma = 3$.

where $E_{g0} = 1.206$ eV [52] is the semiconductor bandgap linearly extrapolated to 0 K, k_B is the Boltzmann constant, q is the elementary charge, and γ is a variable parameter related to recombination [17].

The Suns-V_{OC}(T) measurements reveal the large magnitude of the illumination-intensity-dependent reduction: from around $-0.3\%/°C$ at one-sun to approximately $-0.4\%/°C$ at 0.02 suns, below which the TCs of all cells appear to converge to approximately $-0.6\%/°C$ (at 0.001 suns). The same basic trend has also been observed in multi-crystalline PERC [12] and upgraded metallurgical grade c-Si cells [11]. Above approximately 0.02 suns, the SHJ emerges as the least temperature sensitive of the investigated cells, and the PERC the most temperature sensitive.

Interestingly, these differences seem not to be due to the cells' $TC_{Voc, abs}$, but rather their V_{OC} at 30 °C acting as denominators in calculating TC_{Voc}. The inset to Fig. 4 indicates that the PERC cell has a similar $TC_{Voc, abs}(V_{OC})$ curve as the other homojunction cells. Remarkably, the SHJ is significantly *more* sensitive to temperature than the other cells at the same voltage. This is due to more variable recombination trends in the SHJ cell as characterized by a higher and more varied γ than the other cells (see more in Appendix E).

Above approximately 0.1 suns, the $TC_{Voc}(\phi)$ trend displays a smaller slope due to the larger V_{OC}. The SHJ cell shows more significant bending than the other cells due to its high V_{OC}, resulting in a peak in the difference between the SHJ cell and the other three at approximately 0.2 suns.

One major consequence of the strong dependence of TC_{Voc} on illumination intensity is that V_{OC} calculations based on TC_{Voc} obtained at one-sun will contain misestimations. Fig. 5 shows this expected misestimation as a percentage of the $V_{OC}(\phi, T)$ for the PERC cell. This relative difference is similar across all four investigated cells (see Appendix F). As predicted by Fig. 4, the V_{OC} difference increases from negative to positive as illumination intensity increases past one sun, and the
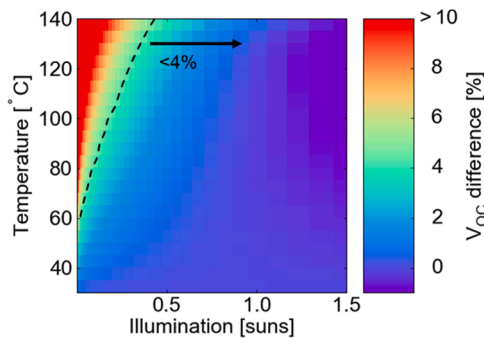
magnitude of the difference below one-sun is higher than the magnitude above. At 90 °C and in the region between 0.5 suns and 1.5 suns, the V_{OC} difference does not exceed 1.2% of the measured value. As typical open field operating conditions around the globe are almost certainly less extreme than these boundaries, $TC_{Voc}(\phi)$ considerations seem to be not of critical importance unless sub-percentage accuracy in voltage or yield estimation is required. However, under conditions of low illumination intensity and high temperature, the misestimation in V_{OC} may exceed 10% (and become as large as 85% near 0.001 suns). This indicates that consideration of $TC_{Voc}(\phi)$ will be crucial for unique low illumination intensity applications of solar cells such as Internet of Things (IoT) in hot environments [53].

3.5. Temperature-dependent local ideality factor

To gain insight into the temperature dependence of the recombination processes, we combined the I-V(T) measurements (at low voltages) and Suns-V_{OC}(T) measurements (at high voltages) of the cut cells and fitted them using the temperature-dependent equivalent-circuit two-diode model [54] at 30 °C and 65 °C. We fit both diode saturation current densities (J_{0x}) at each temperature, along with the temperature-independent diode ideality factor (n) of the second diode. Besides the J-V(T) measurements, m(V, T) – the local slope of the J-V curve (different from the fitted diode ideality factor n[1]) [33] – has been used for the fits. The fitting results are displayed in Table 2, with m(V, T) plotted in Fig. 6. The detailed fitting procedure, along with J-V(T) can be found in Appendix G. Both the low root mean square error (RMSE, normalized at each data point) values, as well as the close visual match, reflect the high quality of fit generated by our model.

An interesting feature in Fig. 6 is the reduction in m(V, T) to below one at higher voltages. For the homojunction cells, it has been proposed that the metal/c-Si interface can be modeled as a Schottky diode in the opposite direction to the p-n junction diode(s), shunted by an ohmic resistance [21,24]. At high illumination intensity (and therefore voltage), the ohmic resistance fails to shunt the Schottky diode, and the Suns-V_{OC} slope increases until a turning point, after which V_{OC} decreases with increasing illumination intensity, and m becomes negative. Due to the high quality of our samples, such a turning point is not seen in the data. Nevertheless, it seems that the Schottky diode model can explain

Table 2
Two-diode model fitting parameters for each cell.

Cell Type	T [°C]	J_{01} [pA/cm²]	J_{02} [nA/cm²]	n_1	n_2	R_{SH} [MΩ•cm²]	RMSE
SHJ	30 °C	0.01 ± 0.00	19.7 ± 4.0	1	2.25	1.3	0.210
	65 °C	2.67 ± 0.56	190 ± 20			0.5	0.167
TOPCon	30 °C	0.17 ± 0.03	2.43 ± 0.45	1	1.8	100	0.139
	65 °C	23.1 ± 3.8	35.5 ± 4.6			100	0.114
PERT	30 °C	0.25 ± 0.04	1.75 ± 0.45	1	1.7	100	0.122
	65 °C	31.8 ± 4.2	28.6 ± 5.6			100	0.097
PERC	30 °C	0.43 ± 0.07	8.5 ± 2.0	1	2	1.5	0.108
	65 °C	61.5 ± 8.5	70.0 ± 19.0			1.2	0.120

Fig. 5. Relative difference between the measured $V_{OC}(\phi, T)$ and the predicted $V_{OC}(\phi, T)$ of the PERC cell using $V_{OC}(\phi, 30 °C)$ and TC_{Voc}(one-sun).

---

[1] In addition to the difference between m and n, it should be noted that n_2 is the *fitted* second diode ideality factor, that is, the value that produces the best fit. In principle, the second diode ideality factor is two.
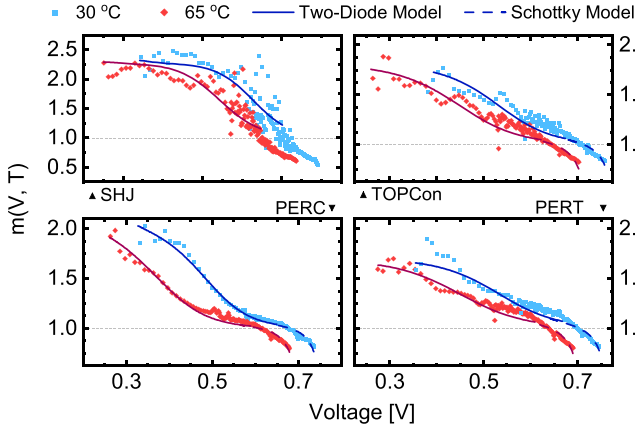
Fig. 6. m(V) of all four cell types at 30 °C and 65 °C, along with curves fitted using the two-diode model (with an additional Schottky diode model for the homojunction cells).

the value of m(V, T) of the homojunction cells at high voltages. For the SHJ cell, although a metal/c-Si interface does not exist, similar mechanisms have been proposed for the c-Si/a-Si interface [55] and the a-Si/TCO interface [56,57]. A combination of these effects, as well as possible contributions from Auger recombination [58] may explain why a single Schottky diode is not sufficient to achieve a reasonable fit for the SHJ cell in this region.

In our implementation of the two-diode model, the only temperature-dependent variables with a significant impact on fitting results are J_{01} and J_{02}. It is widely agreed that J_{01} (n = 1) represents Shockley-Read-Hall (SRH) recombination in the quasi-neutral and surface regions [59,60]. This is consistent with the relative magnitude of J_{01}, which shows that SHJ has the lowest J_{01} and PERC has the highest. On the other hand, J_{02} with $1 < n \leq 2$ is widely attributed to either SRH recombination in the space charge region (SCR) [33,60] or recombination at an exposed section of the p-n junction, known as edge recombination [33,60–62]. For our laser-cleaved cells, edge recombination should constitute a significant portion of this J_{02} current. Additionally, the SHJ cell shows a maximum $n_2 > 2$, which has been well-recorded [63–66], and attributed to heterojunction interface recombination [65,67,68], and hole current saturation in the c-Si at a medium voltage range [66].

Table II shows an approximately 100 times increase of J_{01} between 30 °C and 65 °C for all cell types and approximately 10 times increase for J_{02}. However, it is well-known that due to BGN, the effective intrinsic carrier concentration ($n_{i,eff}$) increases by several orders of magnitude between these temperatures [42]. We therefore normalize J_{01} and J_{02}

with $n^2_{i,eff}$ using the model of Schenk [42,43] at each temperature and cell dopant concentration, and plot the results in Fig. 7, which also contains predictions based on a temperature-dependent J_0 model used by SPICE [69] and adopted by PVsyst [70] and Sandia [71]:

$$\frac{J_0(T_2)}{J_0(T_1)} = \left(\frac{T_2}{T_1}\right)^3 \exp\left\{\frac{1}{nk_B}\left[\frac{E_g(T_1)}{T_1} - \frac{E_g(T_2)}{T_2}\right]\right\} \quad (4)$$

Eq. (4) accounts for changes in n_i^2 and is applicable to J_0 with $n \neq 1$. Fig. 7 shows that, when corrected for $n^2_{i,eff}$, J_{01} appears to decrease by approximately 10% for all three homojunction cells, despite uncertainty ranges extending to breakeven. This indicates the likely existence of a small improvement in bulk and surface passivation for the homojunction cells, which may not be shared by the SHJ cell. In the case of the TOPCon cell, this agrees with the previous report of small improvements in the surface passivation provided by polysilicon passivating contacts [16]. Here, the predictions based on Eq. (4) are close to the $J_{0x,30\,°C}$ = $J_{0x,65\,°C}$ line, verifying the former's effectiveness in adjusting for $n^2_{i,eff}$. For $J_{02}/n^2_{i,eff}$ with $n > 1$, both the fitting results and the predictions based on Eq. (4) show a ten-fold decrease at 65 °C as compared to 30 °C, with the fitting results being lower by 30–50%. This indicates a larger reduction in the recombination processes associated with J_{02} as compared to J_{01}. To our knowledge, the conclusions that the large degrading effect of BGN with increasing temperature obscures a reduction of the c-Si cells' recombination current, and that J_{02} demonstrates a stronger reduction than J_{01} are being reported here for the first time.

4. Conclusions

Using I-V(T), we have characterized the temperature dependence of the main electrical parameters of a range of c-Si cells at one-sun illumination. The TC_{Jsc} of c-Si cells were found to be highly sensitive to spectrum, to the extent that adherence to the I-V testers' A-rating standard does not suffice to produce accurate TC_{Jsc} characterization, producing relative differences to AM1.5G-based TC_{Jsc}'s of up to 30%. In addition, using Suns-V_{OC}(T), we have further characterized the illumination intensity dependence of the cells' TC_{Voc}, which comprises the majority of each cell's TC_{η}. We have found that the TC_{Voc} of all investigated c-Si cells rapidly reduces with decreasing illumination intensity, converging upon approaching 0.001 suns. Above approximately 0.02 suns, the SHJ cell exhibits the best overall TC performance, despite its larger and more varied γ-factor throughout the investigated illumination intensities. Furthermore, modeling of m(V, T) and J-V(T) curves reveal that in all cell types examined, the performance reduction with increasing temperature is overwhelmingly a result of BGN, which is partially offset by reductions in recombination, as reflected in both saturation current densities.
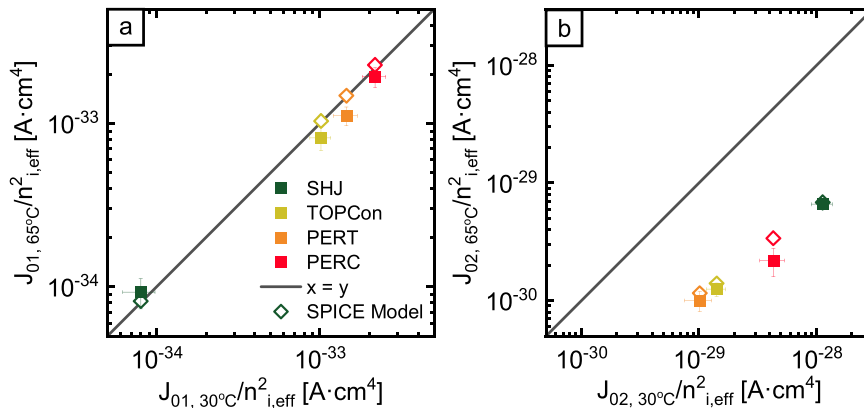

Fig. 7. (a) J_{01} and (b) J_{02} of all four cell types, corrected for $n^2_{i,eff}$, at 30 °C and 65 °C, as well as prediction based on the SPICE model, with the $J_{0x,30\,°C} = J_{0x,60\,°C}$ line as a reference.

The many effects highlighted in this article are expected to be instructive in more than one area of the photovoltaic industry. In solar cell research, the spectral dependences of c-Si cells highlighted by the $EQE(T,\lambda)$ measurements shed light on current matching in two-terminal tandems. In the same area, the SHJ's smaller V_{OC} temperature sensitivity over all field-typical illumination intensities adds valuable data to the investigation of its physical principles. In PV system design, detailed knowledge of the $TC_{Voc}(\phi)$ trend of c-Si cells will lead to an increase in the accuracy of voltage and efficiency predictions. Applied to PV systems in low-illumination, high-temperature regimes such as in certain IoT applications, this will lead to more informed choices regarding technology selection and system sizing.

CRediT authorship contribution statement

Simon M.F. Zhang: Conceptualization, Methodology, Software, Validation, Formal analysis, Investigation, Data curation, Writing – original draft, Writing – review & editing, Visualization, **Johannes P. Seif:** Methodology, Software, Data curation, Writing – review & editing, **Malcolm D. Abbott:** Validation, Writing – review & editing, **Anh Huy Tuan Le:** Methodology, Writing – review & editing, **Thomas G. Allen:** Writing – review & editing, **Ivan Perez-Wurfl:** Methodology, Resources, Supervision, **Ziv Hameiri:** Conceptualization, Methodology, Validation, Resources, Supervision, Project administration, Funding acquisition.

Declaration of Competing Interest

The authors declare that they have no known competing financial interests or personal relationships that could have appeared to influence the work reported in this paper.

Acknowledgement

Appendix A. Supporting information

Supplementary data associated with this article can be found in the online version at doi:10.1016/j.nanoen.2022.107221.

References

[1] VDMA Photovoltaic Equipment, International Technology Roadmap for Photovoltaic (ITRPV) - 2020 Results, 2021.

[2] M.A. Green, Photovoltaic technology and visions for the future, Prog. Energy 1 (2019) 1–13.

[3] J. Haschke, O. Dupré, M. Boccard, C. Ballif, Silicon heterojunction solar cells: Recent technological development and practical aspects - from lab to industry, Sol. Energy Mater. Sol. Cells 187 (2018) 140–153.

[4] F. Feldmann, M. Simon, M. Bivour, C. Reichel, M. Hermle, S.W. Glunz, Carrier selective contacts for silicon solar cells, Appl. Phys. Lett. 104 (2014), 181105.

[5] J. Haschke, J.P. Seif, Y. Riesen, A. Tomasi, J. Cattin, L. Tous, P. Choulat, M. Aleman, E. Cornagliotti, A. Uruena, R. Russell, F. Duerinckx, J. Champliaud, J. Levrat, A.A. Abdallah, B. Aïssa, N. Tabet, N. Wyrsch, M. Despeisse, J. Szlufcik, S. De Wolf, C. Ballif, The impact of silicon solar cell architecture and cell interconnection on energy yield in hot and sunny climates, Energy Environ. Sci. 10 (2017) 1196–1206.

[6] J.P. Seif, G. Krishnamani, B. Demaurex, C. Ballif, S. De Wolf, Amorphous/ crystalline silicon interface passivation: ambient-temperature dependence and implications for solar cell performance, IEEE J. Photovolt. 5 (2015) 718–724.

[7] O. Dupre, R. Vaillon, M.A. Green, Experimental assessment of temperature coefficient theories for silicon solar cells, in: Proceedings of the Forty Second IEEE Photovolt. Spec. Conf., 6 (2015), 56–60. ⟨https://doi.org/10.1109/PVSC.2015. 7355953⟩.

[8] M. Taguchi, E. Maruyama, M. Tanaka, Temperature dependence of amorphous/ crystalline silicon heterojunction solar cells, Jpn, Jpn. J. Appl. Phys. 47 (2008) 814–818.

[9] M. Kasu, J. Abdu, S. Hara, S. Choi, Y. Chiba, A. Masuda, Temperature dependence measurements and performance analyses of high-efficiency interdigitated back-contact, passivated emitter and rear cell, and silicon heterojunction photovoltaic modules, Jpn. J. Appl. Phys. 57 (2018) 08RG18.

[10] I. Bodnár, Electric parameters determination of solar panelby numeric simulations and laboratory measurements during temperature transient, Acta Polytech. Hung. 15 (2018) 59–82.

[11] M. Tayyib, J.O. Odden, T.O. Saetre, Irradiance dependent temperature coefficients for MC solar cells from Elkem solar grade silicon in comparison with reference polysilicon, Energy Procedia 55 (2014) 602–607, https://doi.org/10.1016/j. egypro.2014.08.032.

[12] C. Monokrousso, H. Mullejans, Q. Gao, W. Herrmann, I-V translation procedure for higher accuracy and compliance with PERC cell technology requirements, in: Proceedings of the Thirty Seventh Eur. Photovolt. Sol. Energy Conf. Exhib., 2020, 1120–1125. ⟨https://doi.org/10.4229/EUPVSEC20202020-4AV.2.19⟩.

[13] E. Cuce, P.M. Cuce, T. Bali, An experimental analysis of illumination intensity and temperature dependency of photovoltaic cell parameters, Appl. Energy 111 (2013) 374–382, https://doi.org/10.1016/j.apenergy.2013.05.025.

[14] U. Jahn, M. Schweiger, W. Herrmann, Comparison of different thin-film technologies-performance characteristics obtained from laboratory and field tests, in: Proceedings of the Twenty Fifth Eur. Photovolt. Sol. Energy Conf. Exhib., 2010, 3769–3773. ⟨https://doi.org/10.4229/25thEUPVSEC2010-4BO.10.2⟩.

[15] M. Piliougine, A. Oukaja, M. Sidrach-de-Cardona, G. Spagnuolo, Temperature coefficients of degraded crystalline silicon photovoltaic modules at outdoor conditions, Prog. Photovolt. Res. Appl. 29 (2021) 558–570, https://doi.org/ 10.1002/pip.3396.

[16] A.H.T. Le, R. Basnet, D. Yan, W. Chen, N. Nandakumar, S. Duttagupta, J.P. Seif, Z. Hameiri, Temperature-dependent performance of silicon solar cells with polysilicon passivating contacts, Sol. Energy Mater. Sol. Cells 225 (2021), 111020, https://doi.org/10.1016/j.solmat.2021.111020.

[17] M.A. Green, General temperature dependence of solar cell performance and implications for device modelling, Prog. Photovolt. Res. Appl. 11 (2003) 333–340, https://doi.org/10.1002/pip.496.

[18] C.R. Osterwald, M. Campanelli, T. Moriarty, K.A. Emery, R. Williams, Temperature-dependent spectral mismatch corrections, IEEE J. Photovolt. 5 (2015) 1692–1697, https://doi.org/10.1109/JPHOTOV.2015.2459914.

[19] C.R. Osterwald, M. Campanelli, G.J. Kelly, R. Williams, On the reliability of photovoltaic short-circuit current temperature coefficient measurements, in: Proceedings of the IEEE Forty Second Photovolt. Spec. Conf. PVSC 2015, (2015), 4–9. ⟨https://doi.org/10.1109/PVSC.2015.7355842⟩.

[20] Y. Hishikawa, M. Yoshita, H. Ohshima, K. Yamagoe, H. Shimura, A. Sasaki, T. Ueda, Temperature dependence of the short circuit current and spectral responsivity of various kinds of crystalline silicon photovoltaic devices, Jpn. J. Appl. Phys. 57 (2018) 08RG17, https://doi.org/10.7567/JJAP.57.08RG17.

[21] R.A. Sinton, A. Cuevas, A quasi-steady-state open circuit voltage method for solar cell characterization, in: Proceedings of the Sixteenth Eur. Photovolt. Sol. Energy Conf., Glasgow, 2000, 1152–1155. https://doi.org/citeulike-article-id:6901946.

[22] K.C. Fong, K.R. McIntosh, A.W. Blakers, Accurate series resistance measurements of solar cells, Prog. Photovolt. Res. Appl. 21 (2013) 490–499, https://doi.org/ 10.1002/pip.1216.

[23] R. Dumbrell, M.K. Juhl, T. Trupke, Z. Hameiri, Comparison of terminal and implied open-circuit voltage measurements, IEEE J. Photovolt. 7 (2017) 1376–1383, https://doi.org/10.1109/JPHOTOV.2017.2729889.

[24] S.W. Glunz, J. Nekarda, H. Mäckel, A. Cuevas, Analyzing back contacts of silicon solar cells by Suns-Voc measurements at high illumination densities, in: Proceedings of the Twenty Second Eur. Photovolt. Sol. Energy Conf. Exhib., 2007, 849–853.

[25] A. Straub, R. Gebs, H. Habenicht, S. Trunk, R.A. Bardos, A.B. Sproul, A.G. Aberle, Impedance analysis: a powerful method for the determination of the doping concentration and built-in potential of nonideal semiconductor p-n diodes, J. Appl. Phys. 97 (2005), 083703, https://doi.org/10.1063/1.1868079.

[26] J. Zhao, M. Konig, Y. Yao, Y. Wang, R. Zhou, T. Xie, H. Deng, 24% Silicon heterojunction solar cells on Meyer Burger's on mass production tools and how wafer material impacts cell parameters, in: Proceedings of the Seventh World Conf. Photovolt. Energy Convers. (2018) 1514–1519. ⟨https://doi.org/10.1109/PVSC. 2018.8547908⟩.

[27] S. Chunduri, Status update on heterojunction technology, in: Proceedings of the Taiyang News Webinar Heterojunction Technol, (2019). ⟨https://www.youtube. com/watch?v=oiAPYjTAzZQ⟩. (Accessed 14 April 2021).

[28] Y. Chen, D. Chen, C. Liu, Z. Wang, Y. Zou, Y. He, Y. Wang, L. Yuan, J. Gong, W. Lin, X. Zhang, Y. Yang, H. Shen, Z. Feng, P.P. Altermatt, P.J. Verlinden, Mass production of industrial tunnel oxide passivated contacts (i-TOPCon) silicon solar cells with average efficiency over 23% and modules over 345 W, Prog. Photovolt. Res. Appl. 27 (2019) 827–834, https://doi.org/10.1002/pip.3180.

[29] S. McMahan, imec and its Jolywood achieve 23.2% efficiency with n-PERT solar cells, in: Proceedings of the Eepower, (2019). ⟨https://eepower.com/news/imec-and-its-jolywood-achieve-23-2-efficiency-with-n-pert-solar-cells/⟩. (Accessed 23 September 2021).

[30] R. Chen, H. Tong, H. Zhu, C. Ding, H. Li, D. Chen, B. Hallam, C.M. Chong, S. Wenham, A. Ciesla, 23.83% efficient mono-PERC incorporating advanced hydrogenation, Prog. Photovolt. Res. Appl. 28 (2020) 1239–1247, https://doi.org/10.1002/pip.3243.

[31] S.M.F. Zhang, J.P. Seif, T.G. Allen, R. Basnet, A.H.T. Le, I. Perez-Wurfl, Z. Hameiri, Temperature- and illumination-dependent characterization of solar cells using Suns-Voc(T) and I-V(T), in: Proceedings of the Forty Eighth IEEE Photovolt. Spec. Conf., 2021, 0737–0740.

[32] M.K. Juhl, F.D. Heinz, G. Coletti, D. MacDonald, F.E. Rougieux, F. Schindle, T. Niewelt, M.C. Schubert, An open source based repository for defects in silicon, in: Proceedings of the Seventh World Conf. Photovolt. Energy Convers. (2018) 328–332. https://doi.org/10.1109/PVSC.2018.8547621.

[33] K.R. McIntosh, Lumps, humps and bumps: three detrimental effects in the current-voltage curve of silicon solar cells, Univ. N. South Wales (2001), https://doi.org/10.1007/978-1-349-95810-8_1229.

[34] C.A. Gueymard, SMARTS2: a Simple Model of the Atmospheric Radiative Transfer of Sunshine: Algorithms and Performance Assessment, Cocoa, Florida, 1995, https://doi.org/10.2307/27548210.

[35] M.A. Green, The passivated emitter and rear cell (PERC): from conception to mass production, Sol. Energy Mater. Sol. Cells 143 (2015) 190–197, https://doi.org/10.1016/j.solmat.2015.06.055.

[36] S.W. Glunz, J. Benick, D. Biro, M. Bivour, M. Hermle, D. Pysch, M. Raüer, C. Reichel, A. Richter, M. Rüdiger, C.Schmiga, D. Suwito, A. Wolf, R. Preu, n-type silicon - enabling efficiencies> 20% in industrial production, in: Proceedings of the Thirty Fifth IEEE Photovolt. Spec. Conf. (2010)50–56. ⟨https://doi.org/10.1109/PVSC.2010.5614203⟩.

[37] J. Liu, Y. Yao, S. Xiao, X. Gu, Review of status developments of high-efficiency crystalline silicon solar cells, J. Phys. D. Appl. Phys. 51 (2018), 123001, https://doi.org/10.1088/1361-6463/aaac6d.

[38] M.A. Green, Accuracy of analytical expressions for solar cell fill factors, Sol. Cells 7 (1983) 337–340.

[39] G. Nogay, J.P. Seif, Y. Riesen, A.Tomasi, L. Barraud, N. Wyrsch, F.J. Haug, S. De Wolf, C. Ballif, Microcrystalline silicon carrier collectors for silicon heterojunction solar cells and impact on low-temperature device characteristics, in: Proceedings of the Forty Fourth IEEE Photovolt. Spec. Conf. 6 (2017), 1654–1662. ⟨https://doi.org/10.1109/PVSC.2017.8366840⟩.

[40] J. Peter Seif, A. Descoeudres, M. Filipič, F. Smole, M. Topič, Z. Charles Holman, S. De Wolf, C. Ballif, Amorphous silicon oxide window layers for high-efficiency silicon heterojunction solar cells, J. Appl. Phys. 115 (2014), 024502, https://doi.org/10.1063/1.4861404.

[41] J. Zhao, A. Wang, S.J. Robinson, M.A. Green, Reduced temperature coefficients for recent high-performance silicon solar cells, Prog. Photovolt. Res. Appl. 2 (1994) 221–225, https://doi.org/10.1002/pip.4670020305.

[42] A. Schenk, Finite-temperature full random-phase approximation model of band gap narrowing for silicon device simulation, J. Appl. Phys. 84 (1998) 3684–3695, https://doi.org/10.1063/1.368545.

[43] PV Lighthouse, Bandgap calculator, (n.d.). ⟨https://www.pvlighthouse.com.au/bandgap⟩. (Accessed 17 July 2021).

[44] J.S. Swirhun, R.A. Sinton, M.K. Forsyth, T. Mankad, Contactless measurement of minority carrier lifetime in silicon ingots and bricks, Prog. Photovolt. Res. Appl. 19 (2011) 313–319, https://doi.org/10.1002/pip.

[45] ASTM, Standard Classification for Solar Simulators for Electrical Performance Testing of Photovoltaic Devices, (2019). ⟨https://doi.org/10.1520/E0927-19.2⟩.

[46] F. Martinho, Challenges for the future of tandem photovoltaics on the path to terawatt levels: a technology review, Energy Environ. Sci. 14 (2021) 3840–3871, https://doi.org/10.1039/d1ee00540e.

[47] Q. Xu, Y. Zhao, X. Zhang, Light management in monolithic perovskite/silicon tandem solar cells, Sol. RRL 4 (2020) 1900206, https://doi.org/10.1002/solr.201900206.

[48] C. Messmer, B.S. Goraya, S. Nold, P.S.C. Schulze, V. Sittinger, J. Schön, J. C. Goldschmidt, M. Bivour, S.W. Glunz, M. Hermle, The race for the best silicon bottom cell: Efficiency and cost evaluation of perovskite–silicon tandem solar cells, Prog. Photovolt. Res. Appl. 29 (2021) 744–759, https://doi.org/10.1002/pip.3372.

[49] D.J. Friedman, Modelling of tandem cell temperature coefficients, in: Proceedings of the Twenty Fifth IEEE Photovolt. Spec. Conf. (1996) 89–92. ⟨https://doi.org/10.1109/pvsc.1996.563954⟩.

[50] O. Dupré, R. Vaillon, M.A. Green, Thermal Behavior of Photovoltaic Devices, 2017. ⟨https://doi.org/10.1007/978-3-319-49457-9⟩.

[51] E. Aydin, T.G. Allen, M. De Bastiani, L. Xu, J. Ávila, M. Salvador, E. Van Kerschaver, S. De Wolf, Interplay between temperature and bandgap energies on the outdoor performance of perovskite/silicon tandem solar cells, Nat. Energy 5 (2020) 851–859, https://doi.org/10.1038/s41560-020-00687-4.

[52] M.A. Green, K.A. Emery, A.W. Blakers, Silicon solar cells with reduced temperature sensitivity, Electron. Lett. 18 (1982) 97–98.

[53] R. Haight, W. Haensch, D. Friedman, Solar-powering the internet of things, Science 353 (2016) 124–125, https://doi.org/10.1126/science.aag0476.

[54] M. Wolf, H. Rauschenbach, Resistance effects on measurements, Adv. Energy Convers. 3 (1963) 455–479.

[55] R.V.K. Chavali, J.V. Li, C. Battaglia, S. De Wolf, J.L. Gray, M.A. Alam, A generalized theory explains the anomalous Suns-Voc response of Si heterojunction solar cells,

IEEE J. Photovolt. 7 (2017) 169–176, https://doi.org/10.1109/JPHOTOV.2016.2621346.

[56] M. Bivour, M. Reusch, S. Schroer, F. Feldmann, J. Temmler, H. Steinkemper, M. Hermle, Doped layer optimization for silicon heterojunctions by injection-level-dependent open-circuit voltage measurements, IEEE J. Photovolt. 4 (2014) 566–574, https://doi.org/10.1109/JPHOTOV.2013.2294757.

[57] M. Bivour, C. Reichel, M. Hermle, S.W. Glunz, Improving the a-Si:H(p) rear emitter contact of n-type silicon solar cells, Sol. Energy Mater. Sol. Cells 106 (2012) 11–16, https://doi.org/10.1016/j.solmat.2012.06.036.

[58] A. Richter, S.W. Glunz, F. Werner, J. Schmidt, A. Cuevas, Improved quantitative description of Auger recombination in crystalline silicon, Phys. Rev. B Condens. Matter Mater. Phys. 86 (2012), 165202, https://doi.org/10.1103/PhysRevB.86.165202.

[59] W. Shockley, W.T. Read, Statistics of the recombinations of holes and electrons, Phys. Rev. 87 (1952) 835–842, https://doi.org/10.1103/PhysRev.87.835.

[60] O. Breitenstein, Understanding the current-voltage characteristics of industrial crystalline silicon solar cells by considering inhomogeneous current distributions, Opto Electron. Rev. 21 (2013) 259–282, https://doi.org/10.2478/s11772.

[61] A. Fell, J. Schön, M. Müller, N. Wöhrle, M.C. Schubert, S.W. Glunz, Modeling edge recombination in silicon solar cells, IEEE J. Photovolt. 8 (2018) 428–434, https://doi.org/10.1109/JPHOTOV.2017.2787020.

[62] J. Wong, R. Sridharan, V. Shanmugam, Quantifying edge and peripheral recombination losses in industrial silicon solar cells, IEEE Trans. Electron Devices 62 (2015) 3750–3755, https://doi.org/10.1109/TED.2015.2480089.

[63] M. Taguchi, A. Yano, S. Tohoda, K. Matsuyama, Y. Nakamura, T. Nishiwaki, K. Fujita, E. Maruyama, 24.7% record efficiency HIT solar cell on thin silicon wafer, IEEE J. Photovolt. 4 (2014) 96–99, https://doi.org/10.1109/JPHOTOV.2013.2282737.

[64] F. Gérenton, J. Eymard, S. Harrison, R. Clerc, D. Muñoz, Analysis of edge losses on silicon heterojunction half solar cells, Sol. Energy Mater. Sol. Cells 204 (2020), 110213, https://doi.org/10.1016/j.solmat.2019.110213.

[65] A. Kassis, M. Saad, Analysis of multi-crystalline silicon solar cells at low illumination levels using a modified two-diode model, Sol. Energy Mater. Sol. Cells 94 (2010) 2108–2112, https://doi.org/10.1016/j.solmat.2010.06.036.

[66] R.V.K. Chavali, J.R. Wilcox, B. Ray, J.L. Gray, M.A. Alam, Correlated nonideal effects of dark and light I-V characteristics in a-Si/c-Si heterojunction solar cells, IEEE J. Photovolt. 4 (2014) 763–771, https://doi.org/10.1109/JPHOTOV.2014.2307171.

[67] M. Saad, A. Kassis, Effect of interface recombination on solar cell parameters, Sol. Energy Mater. Sol. Cells 79 (2003) 507–517, https://doi.org/10.1016/S0927-0248(03)00101-6.

[68] H. Bayhan, A.S. Kavasoğlu, Tunnelling enhanced recombination in polycrystalline CdS/CdTe and CdS/Cu(In,Ga)Se2 heterojunction solar cells, Solid State Electron. 49 (2005) 991–996, https://doi.org/10.1016/j.sse.2005.03.012.

[69] G. Massobrio, P. Antognetti. Semiconductor device modelling with SPICE, second ed., McGraw-Hill, New York, 1993.

[70] A. Mermoud, T. Lejeune, Performance assessment of a simulation model For PV modules of any available technology, in: Proceedings of the Twenty Fifth Eur. Photovolt. Sol. Energy Conf. Exhib., (2010), 6–10.

[71] W. De Soto, S.A. Klein, W.A. Beckman, Improvement and validation of a model for photovoltaic array performance, Sol. Energy 80 (2006) 78–88, https://doi.org/10.1016/j.solener.2005.06.010.

Simon M.F. Zhang is a Ph.D. candidate at the School of Photovoltaics and Renewable Energy Engineering at the University of New South Wales in Sydney, Australia, where he also received his Bachelor's degree in Photovoltaics Engineering in 2019. His research interests include the field performance characterization of tandem cells and their component technologies: crystalline silicon, chalcogenide, III-V, and perovskites, as well the high-temperature performance of other module components, and the field degradation of silicon modules.

Johannes P. Seif received his Master degree in Physics from ETH Zurich in 2009 and graduated with a Ph.D. from EPF Lausanne in 2015. During his time in academic research and in industry (Meyer Burger Research and INDEOtec), he worked on crystalline silicon solar cells, mainly silicon heterojunctions (SHJ), while focusing on plasma enhanced chemical vapor deposition (PECVD) process development. After a postdoc at UNSW, Sydney, where he developed PECVD processes for transition metal oxides, he joined Fraunhofer ISE, Freiburg. There he currently develops PECVD processes for both SHJ and tunnel oxide passivating contact solar cells.

Anh Huy Tuan Le is currently a Ph.D. candidate at the School of Photovoltaic and Renewable Energy Engineering, the University of New South Wales, Sydney, Australia. He received a bachelor's degree in materials science from the University of Science, Vietnam National University – Ho Chi Minh City, Vietnam. Afterward, he received a master's degree in electrical and computer engineering from Sungkyunkwan University, South Korea. His research interests include silicon solar cells, passivating contacts, transition metal oxides, temperature- and illumination-dependent performance of solar cells.

Ivan Perez-Wurfl is a senior lecturer and researcher at the School of Photovoltaic and Renewable energy engineering at UNSW. Ivan's main areas of expertise are solar cell design, fabrication and characterization. In particular, he has extensively studied and developed Silicon Quantum Dot solar cells and multijunction SiGe/GaAsP tandem solar cells. Before moving to Australia he worked as a device scientist at Power Sicel Inc (now part of Microsemi Corporation), developing SiC High Power RF devices. He was a Fulbright fellow from 1996 to1999 at the University of Colorado at Boulder where he obtained his PhD in Electrical Engineering in 2002.